



Article

Design of Nano-Catalyst for Removal of Phenolic Compounds from Wastewater by Oxidation Using Modified Digital Basket Baffle Batch Reactor: Experiments and Modeling

Amer T. Nawaf¹, Jasim I. Humadi¹ , Aysar T. Jarullah², Mustafa A. Ahmed³, Shymaa Ali Hameed² and Iqbal M. Mujtaba^{4,*} 

- ¹ Petroleum and Gas Refinery Engineering Department, College of Petroleum Process Engineering, Tikrit University, Tikrit P.O. Box 42, Iraq; amer.talal@tu.edu.iq (A.T.N.); jasim_alhashimi_ppe@tu.edu.iq (J.I.H.)
- ² Chemical Engineering Department, College of Engineering, Tikrit University, Tikrit P.O. Box 42, Iraq; a.t.jarullah@tu.edu.iq (A.T.J.); sh.a.hamed@tu.edu.iq (S.A.H.)
- ³ Ministry of Oil, North Refineries Company, Baiji Refinery, Tikrit P.O. Box 42, Iraq; eng.mustafa.alhamidy@gmail.com
- ⁴ Department of Chemical Engineering, Faculty of Engineering & Informatics, University of Bradford, Bradford BD7 1DP, UK
- * Correspondence: i.m.mujtaba@bradford.ac.uk

Abstract: Removal of phenol and phenolic compounds from wastewater using various techniques has received considerable attention in recent years. In this work, the removal of phenol from a model solution of phenol via catalytic oxidation is investigated with oxidant H_2O_2 . For this purpose, we designed a new nano-catalyst (8% Fe_2O_3/AC) by loading iron oxide nanoparticles over nano-activated carbon via the impregnation process. We modified the recently developed digital basket baffle batch reactor (DBBBR) and used it for the catalytic oxidation process in order to examine the activity of the prepared nano-catalyst. The highest efficiency of phenol removal was found to be 95.35% under the following parameters: oxidation time of 120 min, oxidation temperature at 85 °C, and stirrer speed of 600 rpm. The minimization of the sum of the squared error between the experimental data and predicted results of phenol removal was considered as a base for the optimization technique to estimate the optimal parameters for the kinetic process. The predicted conversion of phenol excellently agreed with the experimental results (absolute average errors < 5%) for a wide range of process parameters.

Keywords: catalytic phenol oxidation; DBBBR; Fe_2O_3/AC ; oxidant (H_2O_2); mathematical modeling



Citation: Nawaf, A.T.; Humadi, J.I.; Jarullah, A.T.; Ahmed, M.A.; Hameed, S.A.; Mujtaba, I.M. Design of Nano-Catalyst for Removal of Phenolic Compounds from Wastewater by Oxidation Using Modified Digital Basket Baffle Batch Reactor: Experiments and Modeling. *Processes* **2023**, *11*, 1990. <https://doi.org/10.3390/pr11071990>

Academic Editor: George Z. Kyzas

Received: 22 May 2023

Revised: 26 June 2023

Accepted: 27 June 2023

Published: 1 July 2023



Copyright: © 2023 by the authors. Licensee MDPI, Basel, Switzerland. This article is an open access article distributed under the terms and conditions of the Creative Commons Attribution (CC BY) license (<https://creativecommons.org/licenses/by/4.0/>).

1. Introduction

Phenol, an essential chemical, is utilized in the production of drugs, fungicides, and preservatives and is also an essential product of the petroleum industry. Nevertheless, phenolic compounds are major contaminants that are categorized as carcinogenic and teratogenic materials [1,2]. These compounds are fed into the environment by several industrial facilities such as the oil, polymer, petrochemical, pharmaceutical, paint, and dye industries [3–5]. Because water is a scarce commodity around the globe, it is essential to remove toxic contaminants such as phenol from wastewater to reclaim and reuse wastewater. Several techniques have been adopted in recent years to remove phenol or phenolic compounds from wastewater [6].

High acidity, salinity, low biodegradability, and chemical oxygen demand (COD) are the major properties for phenolic compounds [4]. Also, low volatilities and readily formed azeotropes and eutectics are important characterizations for these compounds [5]. Therefore, conventional treatment techniques, such as physical and biological methods, have difficulty treating phenol and its derivatives efficiently [1,6]. The catalytic oxidation processes utilizing oxygen, ozone, hydrogen peroxide (H_2O_2), or the combination of them

proved to be a highly efficient process in the elimination of phenolic compounds [7]. Catalytic oxidation employing H_2O_2 is a more environmentally friendly and efficient process as compared with catalytic oxidation utilizing air, since H_2O_2 is a stronger oxidizing agent [8,9]. In this process, phenolic compounds are oxidized by H_2O_2 to water, carbon dioxide, or some short-chain acids in the presence of a catalyst under a moderate operating condition. H_2O_2 is a non-toxic oxidant, promotes the efficiency of the oxidation process, produces green byproducts, and reduces the severe operating conditions of the process. The catalytic wastewater treatment processes via oxidation are implemented employing catalysts, which leads to a reduction in the activation energy and, thus, the process takes place under mild conditions. In addition, H_2O_2 is used as an oxidant in the catalytic oxidation process in order to overcome the limitations of liquid–gas mass transfer and extremely promote the process's performance [9]. Currently, nanomaterials are widely applied in various fields of environmental treatment owing to their unique physiochemical properties. Economically, nanotechnology is beneficial for the utilization of water resources and the conservation of energy. Nanostructured adsorbents are also employed for the treatment of wastewater, as they react at a faster rate and exhibit much higher efficiency [10]. Activated carbons (ACs) are appropriate materials for a wide field of catalytic industries, either as catalysts or catalyst support. The effectiveness of them is considerably affected by their porous structure, surface area, and the surface active sites, which have a significant role in pollutants' removal activity. The resistance to heat and radiation, cost (relatively cheap), stability in acidic/basic solutions, and good mechanical strength are other significant specifications of these materials. The chemistry of ACs' surface is examined by various oxygen functional groups, like lactones, carbonyls/quinones, carboxylic acids, anhydrides, and phenols. These groups of oxygen can be added or eliminated from the materials' surface via applying the thermal treatments for liquid and gas phases [11]. The nanoparticles of iron oxide (Fe_2O_3) have been gaining the focus of researchers in addressing environmental issues. These materials have high efficiency in removing several categories of pollutants found in water via adsorption and photo-degradation processes. Also, the deterioration of water quality has resulted in the utilization of iron oxide nanoparticles as new adsorbents for wastewater treatment. The large surface-area-to-volume ratio and great biocompatibility allow surface modification and easy separation by employing an external magnetic field of iron oxide nanoparticles, presenting them as excellent adsorbents. It is comparatively low cost, is reusable, and has excellent magnetic properties [8].

In this study, a novel nano-catalyst was prepared using 8% Fe as the active metal and activated carbon (AC) (8% Fe/AC) by employing the Incipient Wetness Impregnation (IWI) method. A digital basket baffled batch reactor (DBBBR) was recently designed by Humadi et al. [11], which was used for oxidative desulfurization of fuel. The DBBBR was found to be more effective than a conventional batch reactor by Humadi et al. In this work, we used a different version of the DBBBR (in terms of the size of different components of the reactor) to facilitate the catalytic oxidation of phenol using hydrogen peroxide. A series of experiments were then carried out in the reactor under various operating conditions and the efficiency of the reactor and the catalyst was then evaluated. A mathematical modeling technique was applied to estimate the best values of kinetic parameters for the catalytic phenol oxidation process. Finally, the optimization process was implemented so as to calculate the optimal parameters for the catalytic phenol oxidation process, at which point the removal of phenol was maximized. The novelty of this work is in conducting the catalytic phenol oxidation process in the recently designed reactor in the presence of a new homemade nano-catalyst (8% Fe/AC). Note that this type of reactor has not been used so far for the oxidation of phenol. Also, the mathematical model was built for the catalytic phenol oxidation process to find the optimal operating condition to maximize the removal of phenolic compounds.

2. Materials Used and Experimental Design

2.1. Material Application

2.1.1. Feedstock

The feedstock was a model wastewater which was prepared by injecting phenol (provided by Alpha Chemika Company—Maharashtra, India, purity of 99%) into demineralized water with a total phenol content of 839 ppm, which refers to the initial phenol concentration in the wastewater.

2.1.2. Ferric Nitrate Nonahydrate

Ferric nitrate nonahydrate ($\text{Fe}(\text{NO}_3)_3 \cdot 9\text{H}_2\text{O}$) (obtained from Himedia, India) was utilized as the active metal in the designed nano-catalyst (8% Fe/AC) with purity 98%.

2.1.3. Activated Carbon (AC)

Commercial AC (Supplied from Alpha Chemika Company—Maharashtra, India) was utilized as catalyst support in the homemade prepared nano-catalyst.

2.1.4. Hydrogen Peroxide (30% H_2O_2)

H_2O_2 (Sigma-Aldrich (Burghausen, Germany), purity above 99.99%) was utilized to oxidize phenol to CO_2 and H_2O .

2.2. Incipient Wetness Impregnation (IWI) Process

Incipient Wetness Impregnation (IWI) [12–16] technology was employed in preparing the novel nano-catalyst. At first, AC was treated and dried so as to eliminate any impurities before being utilized in the IWI process. Physical activation of activated carbon and drying under inert operating conditions were carried out to remove any moisture from porosity before using it in the preparation of the nano-catalyst. Temperature of physical activation was 110°C .

After that, the active metal solution was prepared by treating 2 g (of the metal salt) of active metal ($\text{Fe}(\text{NO}_3)_3 \cdot 9\text{H}_2\text{O}$) with 50 mL of deionized water in a magnetic stirrer with rotational speed of 450 RPM for 1.5 h in order to make sure there was complete dissolution of the active metal in the solvent. The produced materials were then filtered in absence of heating to eliminate any further impurities. The active metal solution was then slowly added to 9.2 g of support (AC) with continuous stirring for 1 h in order to make sure that the dispersion of active metal over the support was completed. Finally, calcination process of the product was performed by utilizing the furnace with a gradual increase in temperature to 150°C for 1.5 h. Then, the temperature of calcination was raised to 350°C for 2 h and finally to 560°C for 1.5 h in order to obtain the nano-catalyst (8% $\text{Fe}_2\text{O}_3/\text{AC}$). Figure 1 illustrates the steps of the homemade nano-catalyst (8% $\text{Fe}_2\text{O}_3/\text{AC}$) preparation using IWI technology.

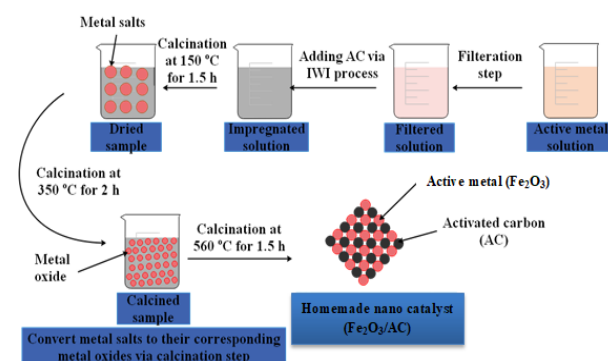


Figure 1. Synthesis of nano-catalyst (8% $\text{Fe}_2\text{O}_3/\text{AC}$) using the IWI process.

2.3. Experimental Procedure

2.3.1. Digital Basket Baffled Batch Reactor (DBBBR)

For the convenience of the readers, we briefly describe the configuration of DBBBR here. The DBBBR was designed in the Petroleum and Gas Refinery Engineering Department, College of Petroleum Process Engineering, Tikrit University/Iraq by Humadi et al. [11] to produce greener fuel by removing sulfur from the fuel via oxidation reaction. In this work, we have redesigned the reactor in terms of different components of the reactor. Evaluation of the effectiveness of the reactor in the context of wastewater treatment via catalytic oxidation process is one of the aims of this work in addition to testing the effectiveness of the new homemade catalyst for such purpose. The design of basket baffled batch reactor enhanced distribution of 8% $\text{Fe}_2\text{O}_3/\text{AC}$ in feedstock and achieved excellent mass transfer rate in the catalytic oxidation process. The DBBBR design involved digital mixer (range of speed from (0 to 5000) RPM), which was linked to a rod, and the end of the rod was connected to the four baskets' impeller. Also, the baskets involved good equal distribution for the circular holes along the baskets' surfaces in a hexagonal form, resulting in mixing channels enhancing inside the catalyst and reactor, thus improving the efficiency of oxidation technology. Four baffles were installed on the reactor wall to minimize stagnant zones in it and promote string of reactants. Baffles were distributed inside the surface of the reactor in equal dimensions (38 cm between every two baffles) and a protrusion of 2.5 cm woolen material (for high temperature conditions above 1000 °C) was used for insulating the reactor. The reactor was made of stainless steel. The specifications of the DBBBR are listed in Table 1 and the schematic of the DBBBR system is illustrated in Figure 2.

Table 1. The specifications of the DBBBR.

Description	Specification
Dimension of reactor	Height = 12 cm, Diameter = 10 m
Length of the rod	37 cm
Type of impeller (Stainless steel)	Four basket impeller
Height of basket	1.2 cm
Length of basket	1.2 cm
Width of basket	1.2 cm
Impeller diameter	94 mm
Height of baffle (Stainless steel)	10 cm
Width of baffle	1.5–1.8 cm

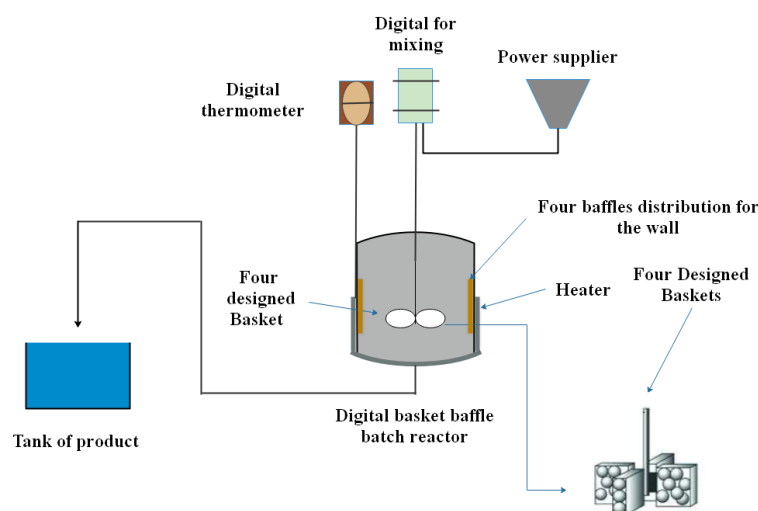


Figure 2. Schematics of the novel digital basket baffle batch reactor system.

2.3.2. Catalytic Oxidation of Phenol Process

In order to examine the performance of the designed nano-catalyst in the modified version of the DBBBR, the catalytic oxidation of phenol used for the model solution of phenol treatment was implemented by using H_2O_2 as oxidant (25 mL fuel/1 mL H_2O_2). Phenol as a model of phenolic compounds was injected in the model solution of phenol with an initial concentration of 839 ppm. The designed 8% $\text{Fe}_2\text{O}_3/\text{AC}$ as charged into the basket with 1.25 g of catalyst in each basket. In the catalytic phenol oxidation process, 100 mL of the feedstock was charged into the DBBBR for each run. For all experiments, the ratio of the amount of feedstock to oxidizing agent (H_2O_2) was 25 and the catalyst weight was 5 g. The catalytic phenol oxidation was processed at mild parameters, where the oxidation time was 30, 60, 90, and 120 min; the reaction temperature was 25, 45, 65, and 85 °C; the magnetic speed was 200, 400, 600, and 800 RPM. Constant pressure of 1 atm was used for all cases. In the chemical reaction, gases were evaporated through the process, which were condensed after that. The treated product was analyzed using a UV spectrophotometer instrument to estimate the final concentration of phenol.

2.3.3. UV Spectrophotometer Analysis

Considering UV-visible spectroscopy was an important suitable technique for determination of phenolic and phenol compounds in model solution. Concentrating the amount of compounds, in fact, depended on two reasons. Firstly, UV light has the ability to absorb phenol and phenolic compounds. Secondly, estimation of the compounds depended on the colored nature that could lead to absorption features in the visible range. The wavelength of phenol was between 210–225 nm.

2.3.4. Characterization of the Prepared Nano-Catalyst (8% $\text{Fe}_2\text{O}_3/\text{AC}$) Brunauer–Emmett–Teller (BET)

Surface area, pore volume, and pore size of the AC support and 8% $\text{Fe}_2\text{O}_3/\text{AC}$ were measured by utilizing the Brunauer–Emmett–Teller (BET) test and the results are explained in Table 2. In the catalytic oxidation process, specific surface area and pore volume of the prepared nano-catalyst (8% $\text{Fe}_2\text{O}_3/\text{AC}$) were very substantial factors influencing the process, where increases in surface area caused enhanced phenol removal. The large surface area contributed to excellent contact area between phenol and H_2O_2 , providing a high rate of elimination of phenol. In addition, the high specific surface area reinforced the diffusion of phenol molecules to the surface-active sites of the catalyst [17].

Table 2. BET results for AC and prepared nano-catalyst.

Property	Support (AC)	Nano-Catalyst (8% $\text{Fe}_2\text{O}_3/\text{AC}$)
Surface area, m^2g^{-1}	908.880	778.107
Total pore volume, cm^3g^{-1}	0.512	0.4416
Mean pore diameter, nm	2.255	2.3824

Scanning Electron Microscope with Energy Dispersive X-ray (SEM-EDX)

The SEM image of 8% $\text{Fe}_2\text{O}_3/\text{AC}$ is displayed in Figure 3A and Table 3. As shown in the figure, a high and excellent distribution of Fe_2O_3 over the AC surface was noticed, where metal oxide is represented by the white regions while AC support is represented by the dark regions. The results of EDX obviously show the elemental composition of the designed nano-catalyst, as illustrated in Figure 3B. The percentage compositions were 10.46%, 26.80%, and 57.77% for iron (Fe), oxygen (O), and carbon (C), respectively. The EDX image displays a regular and good dispersion of active metal on the surface of the nano-catalyst. The results are in good agreement with the theoretical calculations of Fe amount in the designed nano-catalyst.

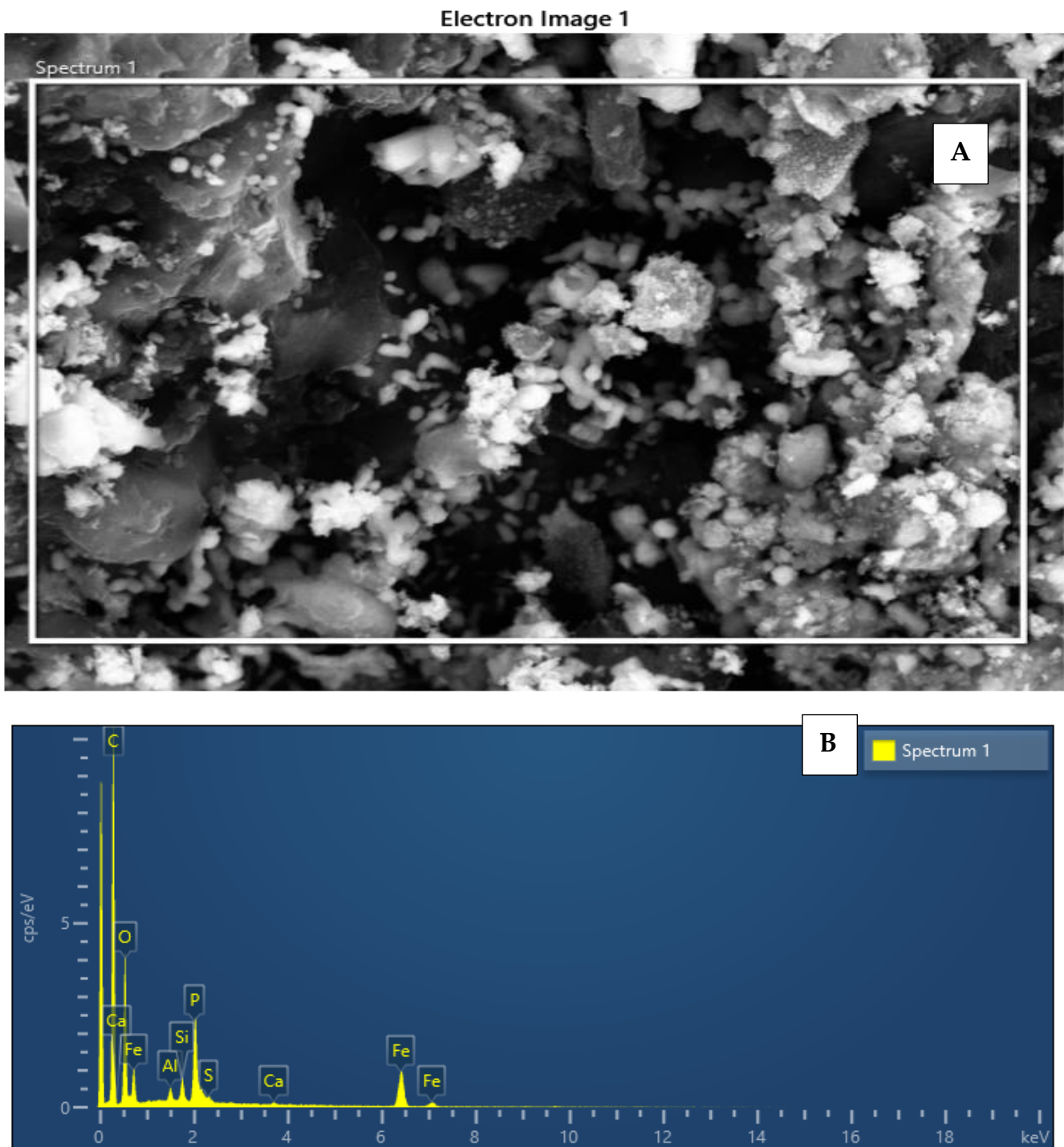


Figure 3. SEM images (A) and EDX (B) for the designed nano-catalyst (8% Fe₂O₃/AC).

Table 3. The amount of element on nano-catalyst.

Element	Line Type	Weight %	Weight % Sigma	Atomic %
C	K series	57.77	0.35	70.37
O	K series	26.80	0.33	24.51
Fe	K series	10.46	0.19	2.74

Fourier Transform Infrared (FTIR) Spectroscopic Analysis

The FTIR test spectrum displays the functional groups of the AC and 8% Fe₂O₃/AC, as referred to in Figure 4. The band at ~3450 cm⁻¹ was ascribed to O-H stretching vibration of hydroxyl groups. The bands at 1650–1500 cm⁻¹ were attributed to an aromatic C=C ring stretching [18]. The absorption band at 1350 cm⁻¹ was attributed to the C-H asymmetric and symmetric bending and the band between 1178 and 1088 cm⁻¹ to the C-O [19]. The absorption peaks at 700–400 cm⁻¹ corresponded to C-C bond stretching vibration [19]. After the loading process of Fe₂O₃ over AC, the absorption bands at ~470 cm⁻¹ and ~550 cm⁻¹ were increased, which was ascribed to Fe–O stretching [20,21].

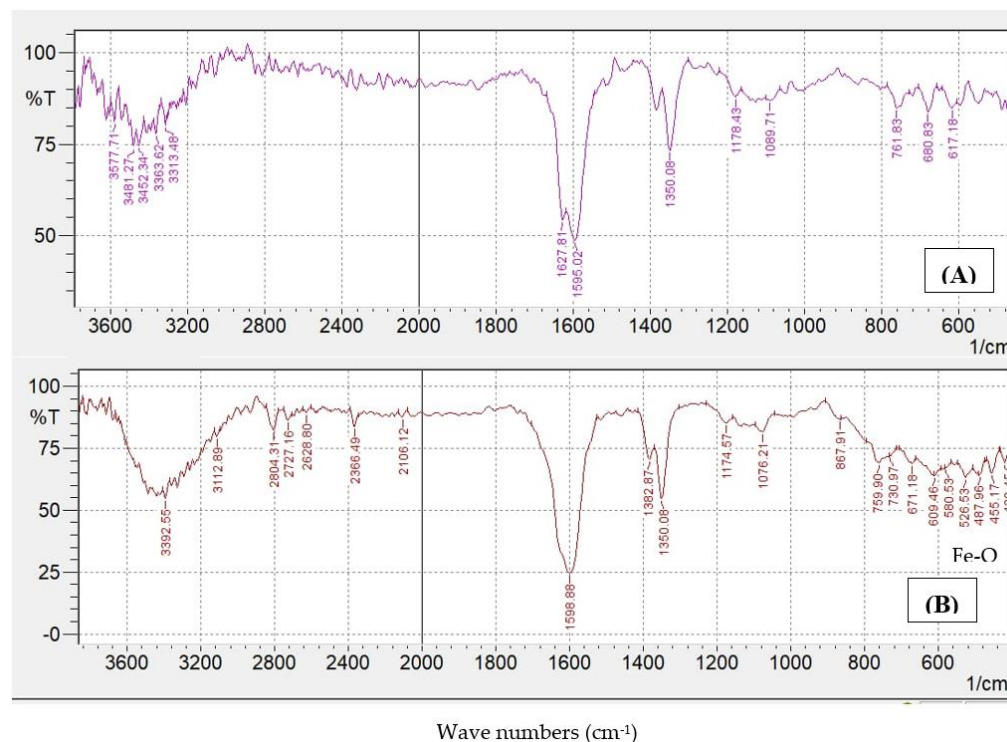


Figure 4. FTIR for (A) activated carbon (AC) and (B) nano-catalyst (8% Fe₂O₃/AC).

3. Results and Discussion

3.1. Effect of Operating Conditions on the Catalytic Oxidation of Phenol

3.1.1. Effect of Stirrer Speed

To investigate the effect of stirrer speed on the efficiency of the phenol oxidation process, several experiments were carried out at different speed such as 200, 400, 600, and 800 RPM; at constant pressure; at different reaction times such as 30, 60, 90, and 120 min; and at different reaction temperatures such as 25, 45, 65, and 85 °C using designed catalyst (8% Fe₂O₃/AC) and H₂O₂ as an oxidant. Figure 5A–D illustrates the impact of stirrer speed on phenol removal for various operating conditions. Clearly, for each set of operating conditions, it was noted that the higher the stirrer speed the higher the conversion of phenol was, except in Figure 5D. The conversion of phenol increased from 80.45% to 94.16% (Figure 5D) when the speed was increased from 200 to 800 RPM with the time of 120 min and temperature of 85 °C [22]. However, the maximum removal of phenol was 95.35% at the best parameters (120 min, 85 °C, and 600 RPM). The influence of mixing intensity had good activity for the dispersion of the catalyst and provided excellent performance in the oxidation of phenol using H₂O₂ oxidant. When the stirrer speed was increased above 800 RPM and the temperature beyond 65 °C, the conversion of phenol decreased due to random mixing which affected the conversion of phenol.

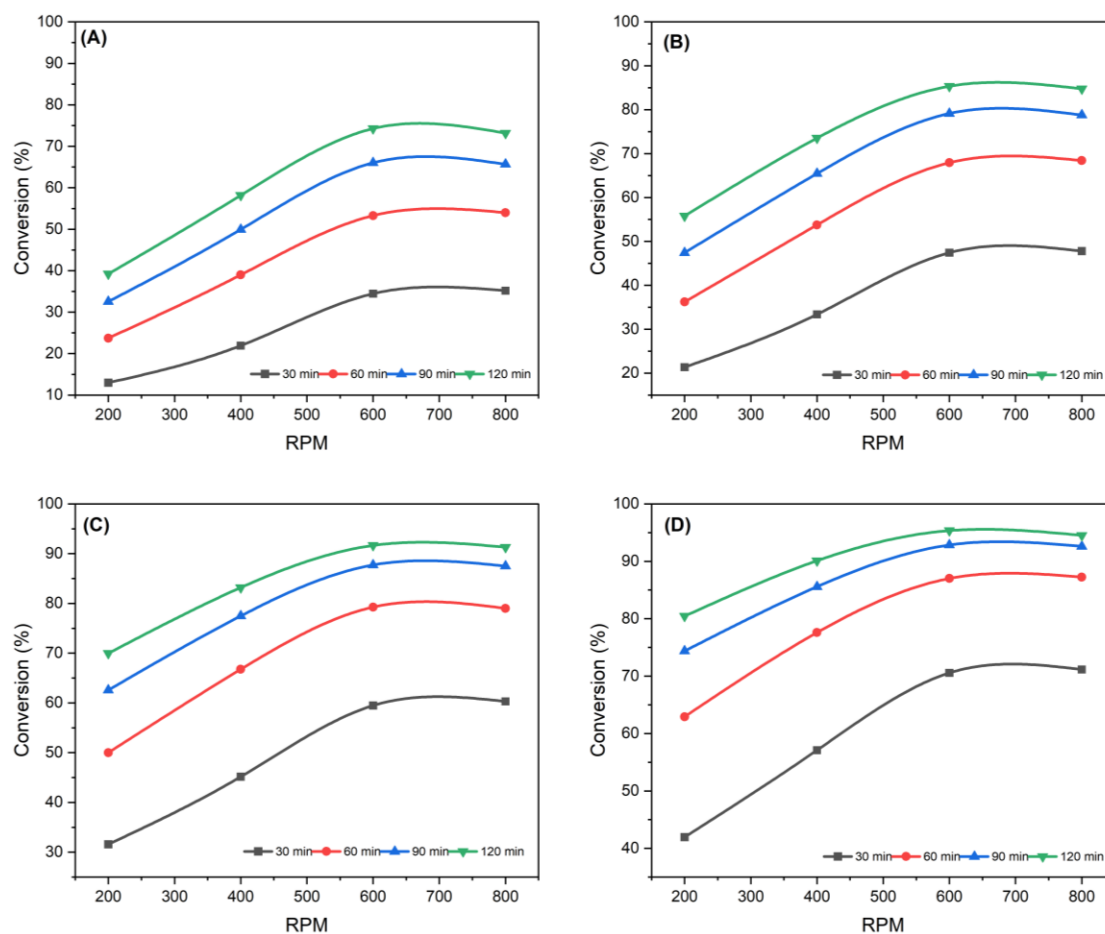


Figure 5. Effect of mixing speed on the removal of phenol process using (8%Fe₂O₃/AC) at different reaction times (30, 60, 90, and 120) min and at (A) 25 °C, (B) 45 °C, (C) 65 °C, and (D) 85 °C.

3.1.2. Effect of Reaction Time

The impact of reaction time on phenol removal is shown in Figure 6A–D at different operating conditions. Figure 6A–D illustrates the impact of reaction time on the oxidation performance. It can be noticed that phenol removal in the BBBR reactor was dramatically promoted via raising the time of reaction as the phenol removal improved from 83.55% to 95.35% when the reaction time was enhanced from 30 min to 120 min at reaction temperature 85 °C and speed of digital 600 RPM, as shown in Figure 6C. This behavior is repeated to improve the time of contacting the oxidant and phenol, consequently supplying sufficient reaction time between phenol and hydroxyl radicals [23,24]. Therefore, oxidation technology needs sufficient time to complete as any other reaction and is improved as time is enhanced. The best oxidation performance was under the oxidation time of 120 min.

3.1.3. Influence of Reaction Temperature

Figure 7A–C shows the effect of temperature on the oxidation of phenol. At different temperatures (25, 45, 65, and 85) °C, the optimal conversion of phenol was 95.35% at the reaction temperature 85 °C. Enhancing the temperature from 25 °C to 85 °C improved the phenol removal from 36.83% to 95.35% at 600 RPM and 120 min. Oxygen free radicals were formed with enhancing temperature, and reacted with oxygen and water to generate H₂O₂ and O₃ [25]. Also, rising temperature improved the number of molecules sharing in oxidizing of phenol via enhancing the activation energy, which improved the phenol and oxygen diffusion inside the catalyst pores [16,17]. Figure 7A–C refers to the impact of the temperature on the phenol oxidation process.

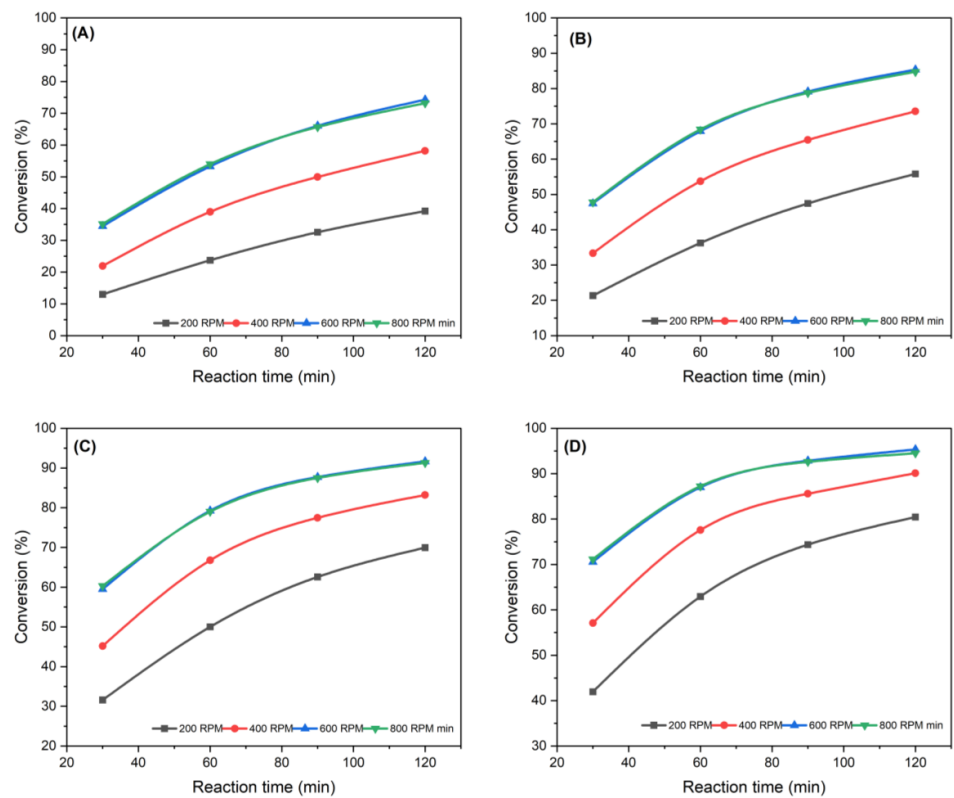


Figure 6. Impact of oxidation time on the removal of phenol process using (8%Fe₂O₃/AC) at different speeds of mixing (200, 400, 600, and 800) min and at (A) 25 °C, (B) 45 °C, (C) 65 °C, and (D) 85 °C.

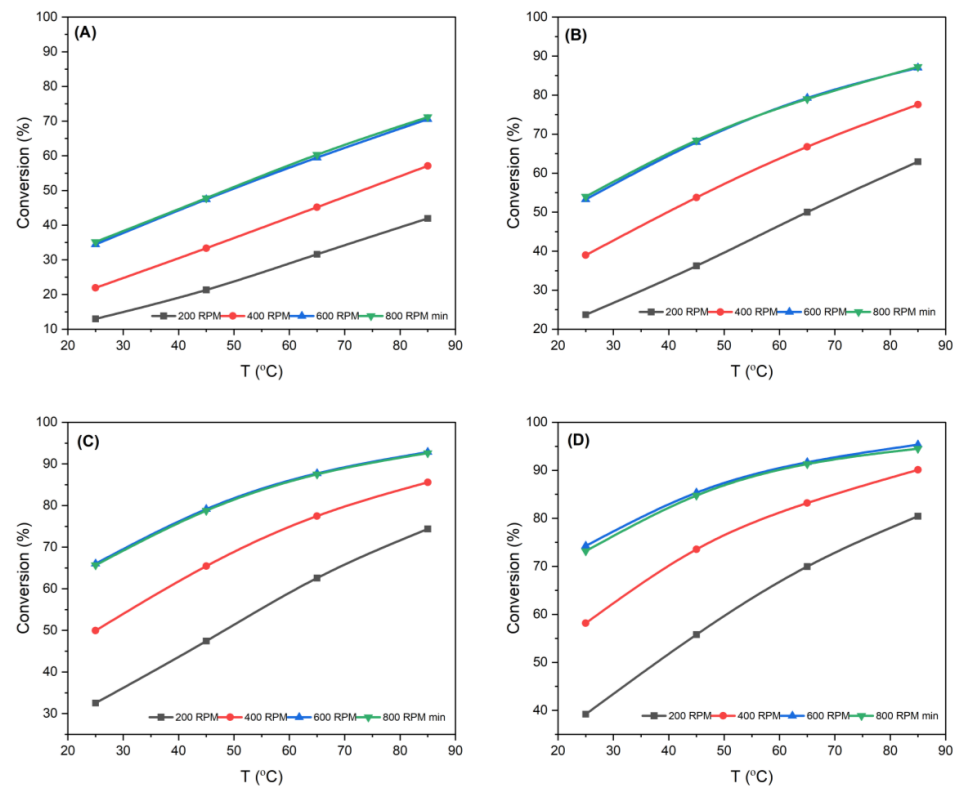


Figure 7. Effect of reaction temperature on the removal of phenol process using (8%Fe₂O₃/AC) at different speeds of mixing (200, 400, 600, and 800) min and at (A) 30 min, (B) 60 min, (C) 90 min, and (D) 120 min.

4. Mathematical Model of DBBBR for Catalytic Phenol Oxidation Process

Mathematical models play a fundamental part in science and engineering in order to reinforce a conception of considerable operations and systems by employing mathematical equations. Mathematical modeling for the catalytic phenol oxidation process was applied by utilizing the gPROMS Version 7.1 (General Process Modeling System) program [14,15]. The equations provided in the mathematical modeling are listed in Table 4 [26–39].

Table 4. The set of equations utilized in the mathematical modeling process.

Parameter (Symbol)	Equations/Values	Equation No.
Rate of reaction ($-r_{ph}$)	$(-r_{ph}) = \eta_0 k C_{ph}^n$	(1)
Arrhenius equation (k)	$k = k_0 e^{(-\frac{E_A}{RT})}$	(2)
The final phenol content (C_{ph})	$C_{ph} = [C_{ph,t}^{(1-n)} + (n-1).t. K_{in} \eta_0]^{(\frac{1}{1-n})}$	(3)
The effectiveness factor (η_0)	$\eta_0 = \frac{3(\phi \coth \phi - 1)}{\phi^2}$	(4)
Thiele modulus (ϕ)	$\phi = \frac{V_p}{S_p} \sqrt{\left(\frac{n+1}{2}\right) \frac{k_{in} C_{ph}^{(n-1)} \rho_p}{D_{ei}}}$	(5)
The catalyst effective diffusivity (D_{ei})	$D_{ei} = \frac{\epsilon_B}{\tau} \frac{1}{\frac{1}{D_{mi}} + \frac{1}{D_{ki}}}$	(6)
The porosity of catalyst (ϵ_B)	$\epsilon_B = V_g \rho_p$	(7)
Particle density (ρ_p)	$\rho_p = \frac{\rho_B}{1 - \epsilon_B}$	(8)
The tortuosity factor (τ)	Tortuosity factor (τ) of the pore network (2 to 7)	---
The Knudsen diffusivity (D_{ki})	$D_{ki} = 9700 r_g \left(\frac{T}{M_{w,ph}}\right)^{0.5}$	(9)
Mean pore radius (r_g)	$r_g = \frac{2V_g}{S_g}$	(10)
The molecular diffusivity (D_{mi})	$D_{mi} = 8.93 * 10^{-8} \left(\frac{v_1^{0.267} T}{v_{ph}^{0.267} \mu_{ph}}\right)$	(11)
The molar volume of the liquid (v_1)	$v_1 = 0.285(v_{cl})^{1.048}$	(12)
The molar volume of the phenol compound (v_{ph})	$v_{ph} = 0.285(v_{cph})^{1.048}$	(13)
The external volume of the catalyst (For sphere particle) (V_p)	$V_p = \frac{4}{3}\pi(r_p)^3$	(14)
The external surface of the catalyst (For sphere particle) (S_p)	$S_p = 4\pi(r_p)^2$	(15)
The phenol viscosity (μ_{ph})	$\mu_{ph} = \exp \left[\ln(\alpha * \mu_{ph,b}) * \frac{\ln(\mu_{ph,b})}{\ln(\alpha * \mu_{ph,b})} \right]^\phi$	(16)
Constant factor (α)	0.1175 for alcohols and 0.248 for other materials.	---
Molecule volume fraction (ϕ)	$\phi = \frac{1-(T/T_c)}{1-(T_b/T_c)}$	(17)

5. Kinetic Parameters Estimation Technique

The kinetic parameters of the catalytic phenol oxidation reaction can be determined by conducting the mathematical modeling process with careful matching of the results of practical experiments with the expected data. In order to estimate the optimal values for kinetic parameters, the minimization of the following objective function was evaluated as summarized below:

$$OBJ = \sum_{n=1}^{Nt} \left(C_{phenol}^{exp} - C_{phenol}^{pred} \right)^2 \quad (18)$$

In Equation (18), Nt is the number of experiments, C_{phenol}^{exp} means the experimental data, and C_{phenol}^{pred} is the mathematical model's results.

The phenol conversion can be calculated using:

$$X_{phenol} = 1 - \frac{C_{phenol}}{C_{phenol,t}} \quad (19)$$

6. Optimization Problem Formulation for Evaluation of Kinetic Parameter

The problem of parameter evaluation was configured as follows:

Given—The conditions of the catalytic phenol oxidation reaction, the catalyst, and the reactor formation.

Obtain—The kinetic parameters (n , k_0 , and EA) for each designed catalyst.

So as to minimize—The sum of squared error (SSE).

Subjected to—Constraints of operation

Mathematically, by counting on the first approach, the optimization problem was presented as follows:

$$\begin{aligned} \text{Min :} & \quad \text{SSE} \\ & \quad n, EA, k_0 \\ \text{S.t.f}(z, x(z), \dot{x}(z), u(z), v) & = 0 \\ & \quad C_L \leq C \leq C_U \\ & \quad n_l \leq n \leq n_u \\ & \quad EA_L \leq EA \leq EA_U \\ & \quad k_{OL} \leq k_i \leq k_{OU} \end{aligned}$$

S.t.f($z, x(z), \dot{x}(z), u(z), v) = 0$: refers to the oxidation process model. z : the independent variable. $u(z)$: the decision variable. $x(z)$: represents the set of all variables. $\dot{x}(z)$: represents the derivative of the variables with respect to time. v : is the control variable. C, C_L, C_U : concentration, lower and upper bounds of concentration. L, U : are lower and upper bounds.

7. Description of Mathematical Modeling

7.1. Determination of Kinetic Parameters

The optimal kinetic parameters of the catalytic phenol removal process were specified by applying the mathematical modeling technique, which minimized the error between the concentrations of phenol resulting from experimental runs and values determined by the model. The constant parameters applied in the modeling technique are reported in Table 5 and the optimal model parameters at various rotation speeds are presented in Tables 6–9.

Table 5. Constant parameters applied in the modeling.

Parameter, Unit	Value
Initial content of phenol (Ct), ppm	839
Reaction time 1, 2, 3, 4, min	30, 60, 90, 120
Reaction temperature (T1, 2, 3, 4), °C	25, 45, 65, 85
R, J/mole.°K	8.314
Vg, cm ³ /gm	0.4536
Sg, cm ² /gm	7,073,700
Vp, cm ³	0.0114137
Sp, cm ²	0.28274
ρ _B , gm/cm ³	1.79377
M.Wt of phenol	184
r _g , nm	1.28249
v _{cl} , cm ³ /gmole	55.95
v _{c,ph} , cm ³ /gmole	229
T _c , °R	1250

Table 6. Oxidation model parameters (Optimal) under 200 RPM.

Parameter	Value
n (-)	1.9997
EA (KJ/mol)	28.8292
k_0 (wt ^{-0.999726} .min ⁻¹)	9989.6200
SSE (-)	1.13996×10^{-5}

Table 7. Oxidation model parameters (Optimal) under 400 RPM.

Parameter	Value
n (-)	1.9869
EA (KJ/mol)	28.1398
k_o (wt ^{-0.999726} .min ⁻¹)	15,712.4700
SSE (-)	7.81139×10^{-6}

Table 8. Oxidation model parameters (Optimal) under 600 RPM.

Parameter	Value
n (-)	1.9265
EA (KJ/mol)	25.6211
k_o (wt ^{-0.999726} .min ⁻¹)	11,854.0200
SSE (-)	7.3293×10^{-6}

Table 9. Oxidation model parameters (Optimal) under 800 RPM.

Parameter	Value
n (-)	1.9629
EA (KJ/mol)	25.9162
k_o (wt ^{-0.999726} .min ⁻¹)	14,265.0800
SSE (-)	7.0075×10^{-6}

7.2. Results of Experiment and Simulation

The experiment's results and predicted data are summarized in Tables 10–13. The generated values of kinetic parameters from ODS modeling give error <5% for all results.

Table 10. Experiment and simulation results under 200 RPM.

Temperature (°C)	Time (min)	Phenol Concentration (ppm)		Conversion %		Error %
		Experimental	Predicted	Experimental	Predicted	
25	30	730	725.39	12.99	13.54	0.63
25	60	640	633.26	23.72	24.52	1.05
25	90	566	558.64	32.54	33.42	1.301
25	120	510	497.62	39.21	40.69	2.43
45	30	660	654.52	21.34	21.99	0.831
45	60	535	523.04	36.23	37.66	2.24
45	90	441	428.62	47.44	48.91	2.81
45	120	371	359.36	55.79	57.17	3.14
65	30	574	570.53	31.59	31.10	0.60
65	60	419	408.45	50.01	51.32	2.52
65	90	314	308.15	62.57	63.27	1.86
65	120	252	243.12	69.96	71.02	3.52
85	30	487	479.45	41.95	42.86	1.56
85	60	311	303.12	62.93	63.88	2.53
85	90	215	211.06	74.37	74.84	1.83
85	120	164	158.26	80.45	81.14	3.50

Table 11. Experiment and simulation results under 400 RPM.

Temperature (°C)	Time (min)	Phenol Concentration (ppm)		Conversion %		Error %
		Experimental	Predicted	Experimental	Predicted	
25	30	655	655.10	21.93	21.81	0.15
25	60	512	524.26	38.98	37.51	2.40
25	90	420	428.99	49.94	48.87	2.14
25	120	351	358.80	58.16	57.24	2.22
45	30	559	564.31	33.37	32.74	0.95

Table 11. Cont.

Temperature (°C)	Time (min)	Phenol Concentration (ppm)		Conversion %		Error %
		Experimental	Predicted	Experimental	Predicted	
45	60	388	398.98	53.75	52.45	2.84
45	90	290	297.35	65.44	64.56	2.53
45	120	222	232.05	73.54	72.34	4.53
65	30	460	464.45	45.17	44.64	0.97
65	60	279	285.33	66.75	65.10	2.27
65	90	189	194.17	77.47	76.86	2.73
65	120	141	143.06	83.19	82.95	1.46
85	30	360	365.53	57.09	56.43	1.54
85	60	188	194.56	77.59	76.81	3.49
85	90	121	122.90	85.58	85.35	1.57
85	120	83	87.07	90.11	89.62	4.90

Table 12. Experiment and simulation results under 600 RPM.

Temperature (°C)	Time (min)	Phenol Concentration (ppm)		Conversion %		Error %
		Experimental	Predicted	Experimental	Predicted	
25	30	550	547.30	34.45	34.77	0.50
25	60	392	375.16	53.28	55.29	4.30
25	90	285	271.57	66.03	67.63	4.71
25	120	216	206.50	74.26	75.39	4.40
45	30	441	422.03	47.44	49.70	4.30
45	60	269	259.08	67.94	69.12	3.69
45	90	175	169.28	79.14	79.82	3.27
45	120	123	120.62	85.34	85.62	1.94
65	30	340	339.86	59.48	59.49	0.04
65	60	174	169.83	79.26	79.76	2.40
65	90	103	102.10	87.72	87.83	0.87
65	120	70	69.65	91.66	91.70	0.50
85	30	247	249.93	70.56	70.21	1.19
85	60	109	108.22	87.01	87.10	0.72
85	90	60	61.44	92.85	92.68	2.40
85	120	39	40.91	95.35	95.12	4.90

Table 13. Experiment and simulation results under 800 RPM.

Temperature (°C)	Time (min)	Phenol Concentration (ppm)		Conversion %		Error %
		Experimental	Predicted	Experimental	Predicted	
25	30	544	522.02	35.16	37.78	4.04
25	60	386	381.91	53.99	54.48	1.06
25	90	288	278.99	65.67	66.75	3.13
25	120	225	213.98	73.18	74.50	4.90
45	30	438	446.77	47.80	46.75	2.00
45	60	265	265.04	68.42	68.41	0.02
45	90	178	175.31	78.78	79.11	1.51
45	120	128	126.32	84.74	84.94	1.31
65	30	333	344.20	60.31	58.98	3.36
65	60	172	174.80	79.50	79.17	1.63
65	90	105	106.76	87.49	87.28	1.68
65	120	73	73.83	91.30	91.20	1.13
85	30	242	253.76	71.16	69.76	4.86
85	60	107	112.24	87.250	86.62	4.90
85	90	62	64.96	92.61	92.26	4.77
85	120	46	43.93	94.52	94.77	4.52

8. Maximizing Phenol Removal Based on Optimal Operating Conditions

8.1. Formulation of Optimization Problem

The optimal kinetic parameters were employed to evaluate the best conditions for achieving the highest elimination of phenol. Therefore, the problem of optimization was created as follows:

Obtain—The optimal parameters for high conversion of phenol compounds.

So as to minimize—The phenol in wastewater.

Subjected to—Constraints in the operation.

The problem was represented mathematically as follows:

$$\begin{aligned}
 & \text{Min} && C_{\text{phenol}} \\
 & T^j, \text{time}_i^j, C_{\text{phenol}}^j, (j = \text{RPM-1, 2, 3, 4}) \\
 & \text{S.t.} && f(z, x(z), \dot{x}(z), u(z), v) = 0 \\
 & && \text{time}_L^j \leq \text{time}^j \leq \text{time}_U^j \\
 & && C_{\text{phenol.tL}}^j \leq C_{\text{phenol.t}}^j \leq C_{\text{phenol.tU}}^j \\
 & && T_L^j \leq T^j \leq T_U^j \\
 & && X_{\text{phenol.tL}}^j \leq X_{\text{phenol.t}}^j \leq X_{\text{phenol.tU}}^j
 \end{aligned}$$

The optimization technique was performed using gPROMS.

8.2. Optimal Values of Operating Conditions for Minimum Phenolic Compounds

The optimal operating conditions determined via using the optimization technique are presented in Table 14.

Table 14. Optimal operating conditions for the oxidation process utilizing the designed catalyst.

Parameter, Unit	Values			
	RPM-1	RPM-2	RPM-3	RPM-4
$C_{\text{phenol.t}}$, ppm	865	864	1104	956
T , °C	77	80	87	81
Time, min	200	193	190	180
Conversion, %	86.99	93.49	98.10	96.99

9. Conclusions

A novel nano-catalyst (8% Fe₂O₃/AC) was designed by employing the impregnated method in order to promote the catalytic phenol oxidation process, which was conducted in a recently developed but modified digital basket baffle batch reactor (DBBBR). There was a high morphology of metal oxide dispersed on the catalyst, as reported by SEM. The phenol oxidation process has shown dependency on the porosity of the prepared nano-catalyst, where such adsorbents' surfaces (activated carbon) have the same base as the active metal oxides (Fe₂O₃). The designed nano-catalyst (8% Fe₂O₃/AC) was found to be a good adsorbent towards the phenolic compound, resulting in elimination of 95.35% phenol at mild operating conditions (reaction temperature 85 °C, reaction time 120 min, and speed of mixing 800 RPM). In the catalytic phenol removal process, it was observed that the utilization of nano-particles for catalyst preparation showed high performance. The IWI impregnation process is a good method for nano-catalyst preparation owing to the excellent dispersion of the active metal beside the high pore volume and surface area of the catalyst (8% Fe₂O₃/AC). The performance of 8% Fe₂O₃/AC depended, fundamentally, on the active compound and the amount of metal oxide loaded over the catalyst support (AC). The minimization of the sum of the squared error between the experimental data and predicted results of phenol removal was considered as a base for the optimization technique to estimate the optimal parameters for the kinetic process. The predicted conversion of

phenol illustrated excellent agreement with the experimental results for a wide range of the operating condition, with absolute average errors less than 5%.

Author Contributions: Conceptualization, A.T.N. and J.I.H.; methodology, M.A.A. and A.T.N.; software, A.T.N. and S.A.H.; validation, A.T.N. and A.T.J.; formal analysis, A.T.N.; investigation, S.A.H. and A.T.N.; resources, M.A.A.; data curation, M.A.A. and J.I.H.; writing—original draft preparation, M.A.A.; writing—review and editing, I.M.M. and A.T.N.; visualization, A.T.N.; supervision, I.M.M. and A.T.N.; project administration, I.M.M. All authors have read and agreed to the published version of the manuscript.

Funding: This research received no external funding.

Data Availability Statement: All data and/or models used in the study appear in the submitted article.

Conflicts of Interest: The authors declare no conflict of interest.

Nomenclature

C_{ph}	Phenol concentration (mol/cm ³)
X_{ph}	Conversion of phenol (-)
C_{ph}	Final concentration of phenol (mol/cm ³)
$C_{ph,t}$	Initial concentration of phenol present in wastewater (mol/cm ³)
k	Reaction rate constant
k_{App}	Apparent rate constant
D_{ei}	Effective diffusivity (cm ² /s)
D_{ki}	Knudsen diffusivity
D_{mi}	Molecular diffusivity (cm ² /s)
EA	Activation energy (J/mol K)
$M_{w,ph}$	Molecular weight of phenol (gm/gmol)
T_c	Critical temperature of phenol (°R)
T_b	Boiling point temperature of phenol (°C)
T_{br}	Reduced boiling point temperature
T_r	Reduced temperature
R	Gas constant (J/mol K)
n	Order of reaction
$-r_{ph}$	Reaction rate of phenol
r_g	Pore radius (nm)
r_p	Particle radius (nm)
S_p	External surface area of catalyst particle (cm ² /gm)
S_g	Specific surface area of particle (cm ²)
V_p	External volume of catalyst particle (cm ³)
V_g	Pore volume (cm ³ /gm)
v_l	Liquid molar volume
v_{cl}	Critical molar volume of liquid (cm ³ /gmole)
v_{ph}	Molar volume of phenol
$v_{c,ph}$	Critical volume of phenol (cm ³ /gmole)

Greek Symbols

η_0	Effectiveness factor
α	Constant factor
Φ	Volume fraction of molecule
\mathcal{E}_B	Porosity
\mathcal{T}	Tortuosity
ρ_B	Bulk density (gm/cm ³)
ρ_p	Particle density (gm/cm ³)
μ_{ph}	Viscosity of phenol (mPa s)
$\mu_{ph,b}$	Viscosity of phenol at boiling point (mPa s)
\circ	Initial (at time = 0)

References

1. Zhang, S.; Zhou, L.; Li, Z.; Esmailpour, A.A.; Li, K.; Wang, S.; Liu, R.; Li, X.; Yun, J. Efficient Treatment of Phenol Wastewater by Catalytic Ozonation over Micron-Sized Hollow MgO Rods. *ACS Omega* **2021**, *6*, 25506–25517. [[CrossRef](#)] [[PubMed](#)]
2. Iurascu, B.; Siminiceanu, I.; Vione, D.; Vicente, M.; Gil, A. Phenol degradation in water through a heterogeneous photo-Fenton process catalyzed by Fe-treated laponite. *Water Res.* **2009**, *43*, 1313–1322. [[CrossRef](#)]
3. Hamad, K.I.; Humadi, J.I.; Issa, Y.S.; Ghani, S.A.; Ahmed, M.A.; Hassan, A.A. Enhancement of activity and lifetime of nano-iron oxide catalyst for environmentally friendly catalytic phenol oxidation process. *Clean. Eng. Technol.* **2022**, *11*, 100570. [[CrossRef](#)]
4. Turhan, K.; Uzman, S. Removal of phenol from water using ozone. *Desalination* **2008**, *229*, 257–263. [[CrossRef](#)]
5. Hamin, J.M.; Aysar, T.J.; Ban, A.A.; Hala, M.H. Preparation of synthetic composite nano-catalyst for oxidative desulfurization of kerosene. *Energy Sources Part A Recovery Util. Environ. Eff.* **2023**, *45*, 1672–1685.
6. Jarullah, A.T.; Ahmed, A.N.; Ahmed, B.A.; Ahmed, A.M. Design of New Composites Nano-Catalysts for Naphtha Reforming Process: Experiments and Process Modeling. *Tikrit J. Eng. Sci.* **2023**, *30*, 46–59. [[CrossRef](#)]
7. Pan, W.; Fang, B.X.; Xin, L.Y. Catalytic oxidation of phenol in wastewater-A new application of the amorphous Fe₇₈Si₉B₁₃ alloy. *Chin. Sci. Bull.* **2012**, *57*, 33–40.
8. Hamoud, S.; Sayari, A.; Belkacemi, K.; Bonneviot, L.; Larachi, F. Catalytic wet oxidation of phenol over Ptx-Ag_{1-x}MnO₂/CeO₂ catalysts. *Catal. Today* **2000**, *62*, 379–388. [[CrossRef](#)]
9. Barrault, J.; Bouchoule, C.; Tatibouët, J.M.; Abdellaoui, M.; Majesté, A.; Louloudi, I.; Papayannakos, N.; Yan, Y.; Wu, X.; Zhang, H. Catalytic wet peroxide oxidation of phenol over Fe₂O₃/MCM-41 in a fixed bed reactor. *Sep. Purif. Technol.* **2016**, *171*, 52–61.
10. Jangid, P.; Inbaraj, M.P. Applications of nanomaterials in wastewater treatment. *Mater. Today Proc.* **2021**, *43*, 2877–2881. [[CrossRef](#)]
11. Humadi, J.I.; Nawaf, A.T.; Jarullah, A.T.; Ahmed, M.A.; Hameed, S.A.; Mujtaba, I.M. Design of new nano-catalysts and digital basket reactor for oxidative desulfurization of fuel: Experiments and modelling. *Chem. Eng. Res. Des.* **2023**, *190*, 634–650. [[CrossRef](#)]
12. Pinho, M.T.; Ribeiro, R.S.; Gomes, H.T.; Faria, J.L.; Silva, A.M.T. Screening of Activated Carbons for the Treatment of Highly Concentrated Phenol Solutions Using Catalytic Wet Peroxide Oxidation: The Effect of Iron Impurities on the Catalytic Activity. *Catalysts* **2020**, *10*, 1318. [[CrossRef](#)]
13. Jain, M.; Yadav, M.; Kohout, T.; Lahtinen, M.; Garg, V.K.; Sillanpää, M. Development of iron oxide/activated carbon nanoparticle composite for the removal of Cr(VI), Cu(II) and Cd(II) ions from aqueous solution. *Water Resour. Ind.* **2018**, *20*, 54–74. [[CrossRef](#)]
14. Nawaf, A.T.; Jarullah, A.T.; Ghani, S.A.; Mujtaba, I.M. Development of Kinetic and Process Models for the Oxidative Desulfurization of Light Fuel, Using Experiments and the Parameter Estimation Technique. *Ind. Eng. Chem. Res.* **2015**, *54*, 12503–12515. [[CrossRef](#)]
15. Jarullah, A.T.; Ahmed, M.A.; Al-Tabbakh, B.A.; Mujtaba, I.M. Design of a new synthetic nanocatalyst resulting high fuel quality based on multiple supports: Experimental investigation and modeling. *Chem. Prod. Process. Model.* **2022**, *18*, 265–293. [[CrossRef](#)]
16. Aabid, A.A.; Humadi, J.I.; Ahmed, G.S.; Jarullah, A.T.; Ahmed, M.A.; Abdullah, W.S. Enhancement of Desulfurization Process for Light Gas Oil Using New Zinc Oxide Loaded Over Alumina Nanocatalyst. *Appl. Sci. Eng. Prog.* **2023**, *16*, 6756. [[CrossRef](#)]
17. Humadi, J.I.; Ghani, S.A.; Ahmed, S.M.R.; Abdullah, G.H.; Phan, A.N.; Harvey, A.P. Fast, non-extractive, and ultra-deep desulfurization of diesel in an oscillatory baffled reactor. *Process Saf. Environ. Prot.* **2021**, *152*, 178–187. [[CrossRef](#)]
18. Saleh, T.A. *Nanotechnology in Oil and Gas Industries: Principles and Applications*; Springer: Cham, Switzerland, 2017.
19. Saka, C. BET, TG-DTG, FT-IR, SEM, iodine number analysis and preparation of activated carbon from acorn shell by chemical activation with ZnCl₂. *J. Anal. Appl. Pyrolysis* **2012**, *95*, 21–24. [[CrossRef](#)]
20. Bakti, A.I.; Gareso, P.L. Characterization of Active Carbon Prepared from Coconuts Shells using FTIR, XRD and SEM Techniques. *J. Ilm. Pendidik. Fis. Al Biruni* **2018**, *7*, 33–39. [[CrossRef](#)]
21. Ramzannezhad, A.; Bahari, A. Characteristics of Fe₃O₄, α-Fe₂O₃, and γ-Fe₂O₃ Nanoparticles as Suitable Candidates in the Field of Nanomedicine. *J. Supercond. Nov. Magn.* **2017**, *30*, 2165–2174.
22. Khoshnam, M.; Farahbakhsh, J.; Zargar, M.; Mohammad, A.W.; Benamor, A.; Ang, W.L.; Mahmoudi, E. α-Fe₂O₃/graphene oxide powder and thin film nanocomposites as peculiar photocatalysts for dye removal from wastewater. *Sci. Rep.* **2021**, *11*, 20378. [[CrossRef](#)] [[PubMed](#)]
23. Kuśmierk, K.; Świątkowski, A. The influence of different agitation techniques on the adsorption kinetics of 4-chlorophenol on granular activated carbon. *React. Kinet. Catal. Lett.* **2015**, *116*, 261–271. [[CrossRef](#)]
24. Humadi, J.I.; Ghani, S.A.; Ahmed, S.M.R.; Harvey, A. Dimensionless evaluation and kinetics of rapid and ultra-deep desulfurization of diesel fuel in an oscillatory baffled reactor. *RSC Adv.* **2022**, *12*, 14385–14396. [[CrossRef](#)] [[PubMed](#)]
25. Ahmed, G.S.; Humadi, J.I.; Aabid, A.A. Mathematical Model, Simulation and Scale up of Batch Reactor Used in Oxidative Desulfurization of Kerosene. *Iraqi J. Chem. Pet. Eng.* **2021**, *22*, 11–17. [[CrossRef](#)]
26. Zazo, J.A.; Pliego, G.; Blasco, S.; Casas, J.A.; Rodriguez, J.J. Intensification of the Fenton process by increasing the temperature. *Ind. Eng. Chem. Res.* **2011**, *50*, 866–870. [[CrossRef](#)]
27. Lann, L.M.V.; Cabassud, M.; Casamatta, G. Modeling, Optimization and Control of Batch Chemical Reactors in Fine Chemical Production. *IFAC Proc. Vol.* **1998**, *31*, 715–724. [[CrossRef](#)]
28. Froment, G.F.; Bischoff, K.B.; Wilde, J.D. *Chemical Reactor Analysis and Design*; Wiley: New York, NY, USA, 1990.
29. Marroquin, G.; Ancheyta, J.; Esteban, C. A batch reactor study to determine effectiveness factors of commercial HDS catalyst. *Catal. Today* **2005**, *104*, 70–75. [[CrossRef](#)]

30. Jarullah, A.T.; Ahmed, G.S.; Al-Tabbakh, B.A.; Mujtaba, I.M. Enhancement of light naphtha quality and environment using new synthetic nano-catalyst for oxidative desulfurization: Experiments and process modeling. *Comput. Chem. Eng.* **2020**, *140*, 106869. [[CrossRef](#)]
31. Humadi, J.I.; Razzaq, G.H.A.; Khamees, L.A.; Ahmed, M.A.; Saeed, L.I. Improved Kerosene Quality with the Use of a Gamma Alumina Nanoparticles Supported Zinc Oxide Catalyst in a Digital Batch Baffled Reactor: Experiments and Process Modelling. *Korean Chem. Eng. Res.* **2023**, *61*, 226–233.
32. Mohammed, A.E.; Jarullah, A.T.; Ghenia, S.A.; Mujtaba, I.M. Optimal design and operation of an industrial three phase reactor for the oxidation of phenol. *Comput. Chem. Eng.* **2016**, *94*, 257–271. [[CrossRef](#)]
33. Duduković, M.P.; Larachi, F.; Mills, P.L. Multiphase catalytic reactors: A perspective on current knowledge and future trends. *Catal. Rev.* **2002**, *44*, 123–246. [[CrossRef](#)]
34. Mohammed, A.E.; Jarullah, A.T.; Ghenia, S.A.; Mujtaba, I.M. Significant Cost and energy Savings Opportunities in industrial three phase reactor for phenol oxidation. *Comput. Chem. Eng.* **2017**, *104*, 201–210. [[CrossRef](#)]
35. Nawaf, A.T. Optimal Kinetic Parameters of Trickle bed Reactor for Oxidation of 2-Propylmercaptan in Naphtha. *Diyala J. Eng. Sci.* **2019**, *12*, 83–100. [[CrossRef](#)]
36. Al-Obaidi, M.A.; Kara-Zaïtri, C.; Mujtaba, I.M. Removal of phenol from wastewater using spiral-wound reverse osmosis process: Model development based on experiment and simulation. *J. Water Process Eng.* **2017**, *18*, 20–28. [[CrossRef](#)]
37. Al-Obaidi, M.A.; Jarullah, A.T.; Kara-Zaïtri, C.; Mujtaba, I.M. Simulation of hybrid trickle bed reactor–reverse osmosis process for the removal of phenol from wastewater. *Comput. Chem. Eng.* **2018**, *113*, 264–273. [[CrossRef](#)]
38. Jarullah, A.T.; Ahmed, A.M.; Hussein, H.M.; Ahmed, A.N.; Mohammed, H.J. Evaluation of synthesized Pt/HY-H- Mor-denite composite catalyst for Isomerization of Light Naphtha. *Tikrit J. Eng. Sci.* **2023**, *30*, 94–103. [[CrossRef](#)]
39. Nawaf, A.T.; Gheni, S.A.; Jarullah, A.T.; Mujtaba, I.M. Optimal Design of a Trickle Bed Reactor for Light Fuel Oxidative Desulfurization Based on Experiments and Modeling. *Energy Fuels* **2015**, *29*, 3366–3376. [[CrossRef](#)]

Disclaimer/Publisher's Note: The statements, opinions and data contained in all publications are solely those of the individual author(s) and contributor(s) and not of MDPI and/or the editor(s). MDPI and/or the editor(s) disclaim responsibility for any injury to people or property resulting from any ideas, methods, instructions or products referred to in the content.